Quantitative Analysis of Cyclic Voltammetry of Redox Monolayers Adsorbed on Semiconductors: Isolating Electrode Kinetics, Lateral Interactions and Diode Currents

Yan B. Vogel[†], Angela Molina[‡], Joaquin Gonzalez*[,‡] and Simone Ciampi*[,†]

[†]Curtin Institute of Functional Molecules and Interfaces, Curtin University, Bentley, Western Australia 6102, Australia

[‡]Departamento de Quimica Fisica, Universidad de Murcia, Murcia 30003, Spain

ABSTRACT: The design of devices whose functions span from sensing their environments, to convert light into electricity or to guide chemical reactivity at surfaces, often hinges around a correct and complete understanding of the factors at play when charges are transferred across an electrified solid/liquid interface. For semiconductor electrodes in particular, published values for charge transfer kinetic constants are scattered. Furthermore, received wisdom suggests slower charge transfer kinetics for semiconductor than for metal electrodes. We have used cyclic voltammetry of ferrocene-modified silicon photoanodes and photocathodes as the experimental model system, and described a systematic analysis to separate charge transfer kinetics from diode effects and interactions between adsorbed species. Our results suggest that literature values of charge transfer kinetic constants at semiconductor electrodes are likely to be an underestimate of their actual values. This is revealed by experiments and analytical models, showing that the description of the potential distribution across the semiconductor/monolayer/electrolyte interface has been largely oversimplified.

Materials that can turn from conductors to insulators are the basis of our digital technology. From the discovery of electrical rectification in galena in 1874,[1] to top-end silicon-based desktop chips,[2] one would be hard-pressed to point to a technologically relevant material that is not a semiconductor.

Where there is the need to gain insights on the "speed" of a charge transfer reaction at a semiconductor/liquid interface, either in energy conversion,[3,4] chemical catalysis[5] or sensing research,[6,7] scientists and engineers require an analytical tool for the kinetic measurement.[8] Cyclic voltammetry is by far the most frequently used technique for such studies; it combines precise and simple control of potential (i.e. thermodynamics of the reaction) with a sensitive measurement of current (i.e. kinetics of the process). Then – to translate experimental numbers into quantitative insights – any given electrochemical measurement needs coupling to a theoretical model.

Mathematical models that are available for the analysis of cyclic voltammetry fall short of capturing all factors at play at the electrified interface: published kinetic data for semiconductors is highly scattered.[9] We believe a contributor to this problem is the naïve character of the available models for kinetics. Kinetic values reported in literature for semiconductor electrodes are usually obtained by analysing cyclic voltammetry data through models that are strictly valid only for metal/liquid interfaces.[10,11] These models are used assuming that under strong illumination a semiconductor behaves like a metal. Such assumption is, in most cases, not valid. Even under strong illumination the electric field inside the semiconductor space charge cannot be completely eliminated. Lewis and co-workers have pioneered a theoretical description of voltammetric curves for redox molecules tethered on semiconductors and accounted for space charge, i.e. diode, effects for the limiting case of reversible electron transfer kinetics.[12] In other words, Lewis and co-workers described the effect semiconductor diode on the shape and position of voltammetric curves but their analysis did not allow to access kinetic parameters.[12] In real systems, beside apparent diode effects that clearly need to be accounted for, the speed of the electron transfer reaction has a finite value. Further, in real systems the current–potential relationship is often complicated by intermolecular and molecule/space charge interactions.[13,14,15,16] We have recently developed an analytical model to interpret cyclic voltammograms by accounting for the semiconducting nature of the electrode, in particular for its electrostatic landscape. We showed that non-idealities, namely full width at half maximum <90.6 mV, and anti-thermodynamic peak positions ($E_{peak\ anodic} < E_{peak\ cathodic}$), are the manifestation of dynamic electrostatic interactions between molecular

charges of a tethered redox probe and the semiconductor space charge.[15]

All this suggests that commonly used models are oversimplified. Particularly, "metallic" models often suggest electron transfer kinetics at semiconductor electrodes being slower than at metallic electrodes.[9] The slower kinetics has been hypothesized to be linked to a poor coupling between energy levels in the electrode and attached molecules, to a low density of states, and to differences in the molecular packing.[9] In the present work we argue that the slower kinetics reported for semiconducting electrodes is in some cases only apparent, and that it might be just a consequence of using models that cannot distinguish between electron transfer kinetic and semiconductor-related effects in the electrochemical response. We describe a model that simulates current–potential traces of cyclic voltammograms for electroactive species adsorbed on semiconductor electrodes, allowing to retrieve kinetic and diode parameters from the fitting of experimental data. This model also allows accounting for i) changes in photocurrents (i.e. open circuit values) between forward and backward sweeps, and ii) attractive and repulsive intermolecular forces sensed by the monolayer. By using this model, we have obtained quantitative insights on the kinetics of a ferrocene monolayer tethered on amorphous silicon photoanodes and photocathodes.

EXPERIMENTAL SECTION

Electrode modification followed a previously reported procedure (details in the Supporting Information).[15] Cyclic voltammograms of ferrocene-modified silicon electrodes were recorded with a CHI650E potentiostat (CH Instruments) and using a three-electrode and single-compartment PTFE cell fitted with an Ag/AgCl (sat. KCl) as the reference electrode and a platinum mesh as the counter electrode. All potentials are reported versus the reference electrode. Ohmic contact to the modified silicon electrode was ensured by using emery paper to grind a thin layer of indium-gallium eutectic on its backside, and then pressing it against a copper plate. A rectilinear cross-section gasket defined the active area of the working electrode to 0.28 cm^2. An aqueous solution of perchloric acid (1.0 M) was used as the electrolyte. Light was shined from the electrolyte side using a red LED (M625L3 source coupled to a SM1P25-A collimator adapter, Thorlabs). The light intensity was regulated through the LED driver (LEDD1B, Thorlabs), and measured with a light meter (LM-200LED, Amprobe). Models and simulations of experimental data were written and performed in GFortran and Mathcad 14.

RESULTS AND DISCUSSION

Development of the analytical model. The voltammetric model described below is applicable to electroactive species attached on a semiconductor electrode and with finite electron transfer kinetics. The electrified semiconductor/monolayer/electrolyte interface is modelled as two polarizable interfaces that are arranged in series: a photodiode in series with an ideal metal electrode with surface-attached redox species that follow Butler-Volmer kinetics (see Figure 1a). A key feature of the model is that it accounts for the balance of intermolecular attractive and repulsive forces (which are often evident in the experiments[14,15,17]), with the thermodynamics of these interactions introduced through the Frumkin isotherm, as well as for dynamic changes in diode parameters from the forward to the backward scan.

The potential, E, is applied between the ohmic back contact made to the semiconductor electrode and the reference electrode. E is distributed between the space charge layer, E_d, and the monolayer/electrolyte interface, E_e:

$$E = E_d + E_e \tag{1}$$

and the current passing through the two interfaces is identical:

$$I = I_d = I_e \tag{2}$$

In order to describe the current–potential (I–E) relationship for this system (Figure 1a) we need to know the I–E expressions for each independent element (i.e. the series arrangement of a photodiode and the monolayer/electrolyte interface). These two elements are described for photoanodes and photocathodes (i.e. monolayer systems tethered on n- and p-type substrates, respectively) by the following:

i. For the first element of the circuit we can use the ideal diode equation for the photodiode steady state I–E relationship, which is given by:

$$I_{\mathrm{d}} = I_{\mathrm{L}} + I_0\left[1-\exp\left(-\frac{nFE_{\mathrm{d}}}{RTD}\right)\right]$$

(photoanode) (3)

$$I_{\mathrm{d}} = I_{\mathrm{L}} + I_0\left[\exp\left(\frac{nFE_d}{RTD}\right)-1\right]$$

(photocathode) (4)

where I_L and I_0 are the photogenerated current and the reverse saturation diode current, and D is the diode ideality factor, which typically varies from 1 to 2. I_L is logically related with the intensity of irradiated light. We could assume that this relationship is linear[18]

through a factor "f_I", i.e., $I_{L,\text{net}} = f_I I_L$, with $0 < f_I < 1$ (lower limit zero corresponds to no illumination and upper limit unity to "full" illumination).

Equations (3) and (4) can be rearranged as:

$$\frac{I_\text{d}}{I_\text{L} + I_0} = 1 - \exp\left[-\frac{nF}{RTD}\left(E_\text{e} - E_{OC}\right)\right]$$

(photoanode) (5)

$$\frac{I_d}{-I_\text{L} + I_0} = \exp\left[\frac{nF}{RTD}\left(E_\text{e} - E_{OC}\right)\right] - 1$$

(photocathode) (6)

where E_{OC} is the open circuit potential given by:

$$E_\text{OC} = \frac{DRT}{nF}\ln\left(\frac{I_0}{I_\text{L} + I_0}\right)$$

(photoanode) (7)

$$E_\text{OC} = \frac{DRT}{nF}\ln\left(\frac{|I_\text{L}| + I_0}{I_0}\right)$$

(photocathode) (8)

ii. The second element of the circuit is equivalent to a redox couple attached onto a metallic electrode. The *I–E* relationship for a cyclic voltammetry experiment when interactions of the attached redox species (in the oxidized, O, and reduced, R, forms) are not negligible was developed by Laviron assuming a Frumkin isotherm:[10,11]

$$I = \frac{1}{nQ_F} k_{red}[\, f_R \mathrm{e}^{\eta_e} \mathrm{e}^{-(y-G)-f_R(G+s)} - \left(1 - f_R\right)\mathrm{e}^{-(y-s)+f_R(G-s)}] \quad (9)$$

where

$$G = a_o + a_r + a_{or} \quad (10)$$

$$s = a_r - a_o \quad (11)$$

$$y = a_o + a_r \quad (12)$$

a_o, a_r and a_{or} are interaction coefficients expressing, respectively, the repulsive O–O and R–R and the attractive O–R interactions. *G* describes the overall interaction, *s* the difference between O–O and R–R interactions, and *y* the overall interaction magnitude. The total amount of charge transferred (in Coulombs) is Q_F , and η_e is defined as:

$$\eta_e = \frac{nF}{RT}\left(E_e - E^{0\prime}\right) \quad (13)$$

with $E^{0\prime}$ being the formal potential of the process and considering the Butler-Volmer kinetic approach, k_{red} is given by:

$$k_{red} = k_{et} e^{-\alpha\eta_e} \quad (14)$$

with k_{et} and α being the conditional rate constant (the value of the rate constant for electro-reduction or electro-oxidation at $E = E^{0\prime}$), and the charge transfer coefficient, respectively.

Equation (9) can be rearranged as:

$$\frac{I}{nQ_F} = k_{\text{et,ap}} \mathrm{e}^{-\alpha\eta_{e,\text{ap}}} e^{-sf_\text{R}} \left(f_\text{R} e^{\eta_{e,\text{ap}}} e^{G(1-f_\text{R})} - \left(1 - f_\text{R}\right) e^{Gf_\text{R}}\right) \quad (15)$$

where

$$\left.\begin{aligned} k_{\text{et,ap}} &= k_{et} e^{s-y} = k_{et} e^{s-G-2a_\text{OR}} \\ \eta_{e,\text{ap}} &= \frac{nF}{RT}\left(E_e - E^{0\prime}_{\text{ap}}\right) \\ E^{0\prime}_{\text{ap}} &= E^{0\prime} + \frac{RT}{nF} s \end{aligned}\right\} \quad (16)$$

$k_{et,\text{ap}}$ is an apparent rate constant and its value changes depending in the values of the interaction parameters.

The current in terms of the variation of f_R , i.e. the changes to the surface coverage of the species *R*, can be written as:

$$\frac{I}{nQ_F} = -v\frac{df_R}{dE_e} \quad (17)$$

where *v* is the scan rate.

Equation (9) can then be re-written in a dimensionless way as follows:

$$\psi = \frac{I}{I_{p,rev}} = -\left(4 - 2G\right)\frac{df_R}{d\eta} = \left(4 - 2G\right)\bar{k}_{red,\text{ap}} \times \times e^{-sf_\text{R}} \left(f_\text{R} e^{\eta_{e,\text{ap}}} e^{G(1-f_\text{R})} - \left(1 - f_\text{R}\right) e^{Gf_\text{R}}\right) \quad (18)$$

with

$$I_{p,rev} = \pm\frac{1}{H}\frac{1}{4 - 2G} \quad (19)$$

$$H = \frac{RT}{n^2 Fv}\frac{1}{Q_F} \quad (20)$$

$$\bar{k}_{red,\text{ap}} = \bar{k}_{\text{et,ap}} \mathrm{e}^{-\alpha\eta} \quad (21)$$

$$\bar{k}_{\text{et,ap}} = k_{\text{et,ap}} / \left(\frac{nFv}{RT}\right) \quad (22)$$

Note that $I_{p,rev}$ given by eq (19) corresponds to the peak potential of a monolayer at a metallic electrode

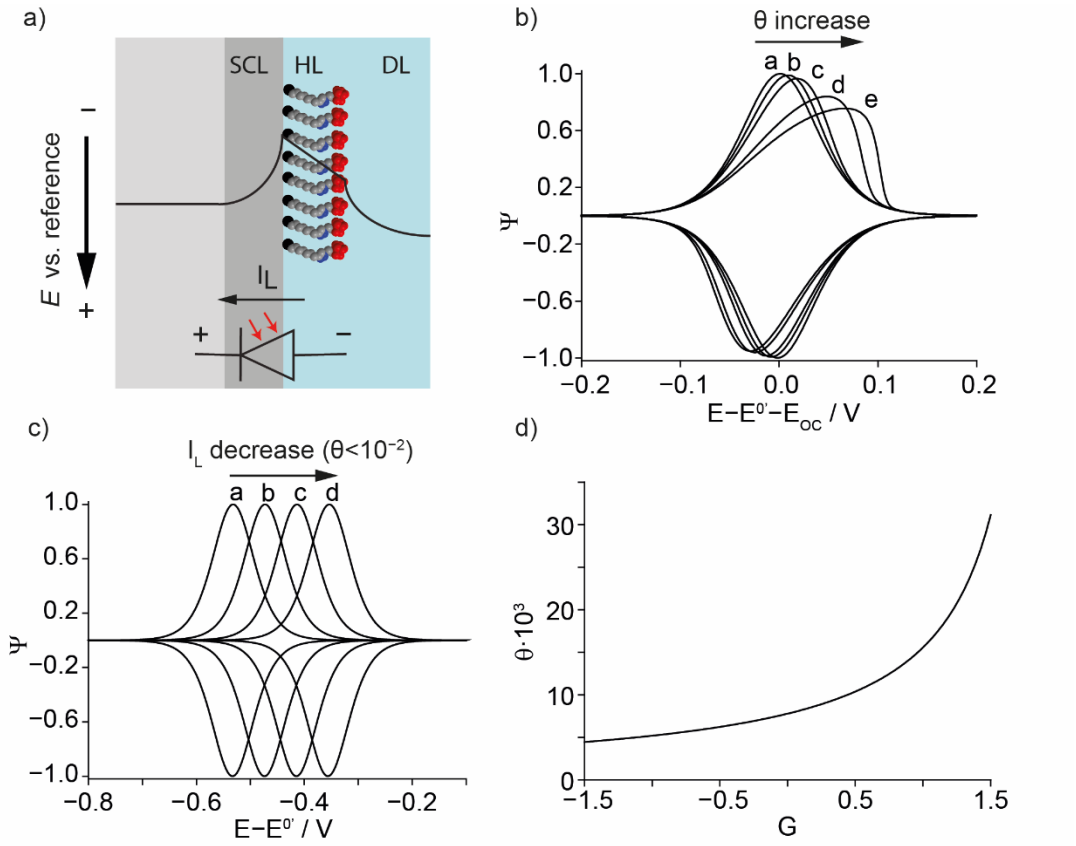

Figure 1. Theoretical landscape and simulated electrochemical responses for the limiting case of reversible kinetics without electrostatic interactions for a photoanode. (a) Representation of the potential drop across the space charge layer (SCL), Helmoltz layer (HL) and double layer (DL). In the model, the potential drop across the SCL behaves as an ideal diode. (b) Shape of the voltammetric curves as a function of θ assuming infinite electron transfer kinetics and neglecting molecular interactions. From **a** to **e** values of θ change from $7.8\cdot10^{-3}$, $7.8\cdot10^{-2}$, 0.156, 0.389 to 0.519. (c) Peak positions depend on the open circuit potential, which is a function of the $I_0/(I_0+I_L)$ ratio (see equation (7). I_0 is 10^{-9} A, v is 0.1 V/s, Q is $8\cdot10^{-6}$ C, and I_L drops progressively from curve **a** to curve **d** (1, 0.1, 0.01 and 0.001 A, respectively). For all the curves $\theta < 10^{-2}$, which results in no changes to the curve shapes. (d) Effect of changes to the interaction parameter on values of θ for a Nernstian charge transfer. Repulsive molecular interactions (negative G) lower θ, and attractive interactions (positive G) increase θ. Sweep rate is 0.1 V/s, Q is $8\cdot10^{-6}$ C, I_L is 1μA, and I_0 is 1×10^{-11} A.

under Nernstian condition, i.e., for a very fast redox conversion of the electroactive couple. It will be used as a reference value.

iii. With eqs (7), (8) and (18) we have the equations necessary to obtain the current–potential expressions for photoanodes and photocathodes:

$$\frac{I_d}{I_{p,rev}} = \frac{1}{\theta}\left\{1-\exp\left[-\frac{nF}{DRT}\left(E_d - E_{OC}\right)\right]\right\}$$

(photoanode) (23)

$$\frac{I_d}{I_{p,rev}} = \frac{1}{\theta}\left\{\exp\left[\frac{nF}{DRT}\left(E_d - E_{OC}\right)\right]-1\right\}$$

(photocathode) (24)

with θ defined as:

$$\theta = \frac{I_{p,rev}}{\left|I_L\right| + I_0} \quad (25)$$

In order to solve eq (18), the values of at least one of the two potential drops, E_e or E_d, have to be determined to calculate $I_{p,rev}$. We can for example work on E_d, which can be obtained from eqs (23) or (24):

$$E_d = E_{OC} - \frac{DRT}{nF}\ln\left(1-\theta\psi\right)$$

(photoanode) (26)

$$E_d = E_{OC} + \frac{DRT}{nF}\ln\left(1+\theta\psi\right)$$

(photocathode) (27)

By taking into account that

$$E_e - E^{0\prime} = E - E^{0\prime} - E_d \quad (28)$$

From eqs (26)–(28) we can write the following:

$$e^{\eta_e} = e^{\eta_{eff}}\left(1-\theta\psi\right)^D \text{ (photoanode)} \quad (29)$$

$$e^{\eta_e} = \frac{e^{\eta_{eff}}}{(1+\theta\psi)^D} \quad \text{(photocathode)} \tag{30}$$

where

$$\eta_{eff} = \frac{nF}{RT}\left(E - E^{0\prime} - E_{OC}\right) \tag{31}$$

By inserting eqs (29) or (30) into (18) two differential equations are obtained:

$$-\frac{df_R}{d\eta} = \bar{k}_{et,ap} e^{-\alpha\eta_{eff}} (1-\theta\psi)^{-\alpha D} e^{-sf_R} \times$$
$$\times\left(f_R e^{G(1-f_R)} e^{\eta_{eff}} (1-\theta\psi)^D - (1-f_R) e^{Gf_R} \right)$$
(photoanode) (32)

$$-\frac{df_R}{d\eta} = \bar{k}_{et,ap} \frac{e^{-\alpha\eta_{eff}}}{(1+\theta\psi)^{-\alpha D}} e^{-sf_R} \times$$
$$\times\left\{ \frac{f_R e^{G(1-f_R)} e^{\eta_{eff}}}{(1+\theta\psi)^D} - (1-f_R) e^{Gf_R} \right\}$$
(photocathode) (33)

Equations (32) and (33) have no algebraic solution and have to be solved numerically. This can be done by using the Euler method for the determination of ψ, for which the derivate in eq (18) can be changed to:

$$\left|\frac{\psi}{4-2G}\right| = \left|\frac{df_R}{d\eta}\right| \approx \left|\frac{\Delta f_R}{\Delta\eta}\right| = \left|\frac{f_{R,i} - f_{R,i-1}}{\Delta\eta}\right| \tag{34}$$

Where the subscript *i* indicates the potential being considered. By inserting eq (34) into eq (32) and eq (33) an algebraic implicit equation is obtained that can be solved by iteration.

Quantitative analysis of an experimental model The potential applied across the semiconductor/molecular monolayer/electrolyte interfaces is distributed between two polarizable interfaces: the semiconductor space charge layer and the molecular monolayer/electrolyte interface. These interfaces can be described by two electrical elements in series: a diode which follows the Shockley relationship (eqs (3) and (4)), and a molecular monolayer of an attached redox molecule with electron transfer kinetics following Laviron's formalism (eq (15)). This is schematically depicted in Figure 1a for a photoanode. The semiconductor potential drop is only a function of the ratio $\theta = I_{p,rev} / (I_0 + I_L)$, where $I_{p,rev}$ is the peak current for a Nernstian process, I_L is the photocurrent and I_0 the reverse saturation current of a diode. Fig. 1b shows simulated cyclic voltammograms for different values of θ in the case of a redox couple under infinitely fast kinetics. The current axis in the simulated voltammograms have been normalized to the dimensionless current ψ (eq(18)) and the abscissa represents the voltage E relative to the redox formal potential $E^{0\prime}$ corrected for the open circuit potential E_{OC} (i.e. $E - E^{0\prime} - E_{OC}$). For θ values lower than ca. 10^{-2} the shape of the curves appear identical to those for metal electrodes. It is evident from Figure 1b (photoanode) thatt the anodic peak is more sensitive to changes in θ than the cathodic peak. For a photocathode the situation is reversed – the cathodic peak is most sensitive to changes in θ. While θ accounts for the shape of the peak, the peak position is defined by E_{OC}, which is a function of the $I_0/(I_0+I_L)$ ratio, as shown in eq (7). Figure 1c shows changes in the peak position as a consequence of changes in the open circuit potential (i.e. changes in the $I_0 / (I_0 + I_L)$ ratio) when $\theta < 10^{-2}$, that is, when the shape of the voltammograms on semiconductors is like that on a metallic electrode.

As discussed above, θ affects the shape of the cyclic voltammogram (for $\theta > 10^{-2}$) and E_{OC} its position, and are ultimately a function of three parameters: $I_{p,rev}$, I_0 and I_L. $I_{p,rev}$ is the peak intensity for a Nernstian process when diode effects are not present and is a function of the scan rate; increasing the scan rate increases $I_{p,rev}$, as is shown in eqs (17) and (18). The magnitude of $I_{p,rev}$ also depends on the interactions – either repulsive or attractive – experienced by the tethered redox centres, through the Frumkin isotherm and its parameter *G:* repulsive interactions will decrease the magnitude of $I_{p,rev}$, attractive interactions will increase it (eqs (17) and (18)). Figure 1d plots the dependence of the diode parameter θ on the interaction parameter *G*, and shows that diode effects are more evident as interactions move in favour to attractions (positive *G*). I_0 is the current under dark conditions and is characteristic for a given system at constant temperature; the higher I_0 the more the system becomes "metallic". The photocurrent, I_L, is linearly and directly dependent on the light intensity[18,19] and diode effects, i.e. effects that make the system become less "metallic" are more relevant at low I_L values (see eq (23)), that is, under low light intensity. As θ depends on $I_{p,rev}$, I_L and I_0 (see eq (25)), the practical challenge resides in determining them separately. $I_{p,rev}$ can be determined in the Nernstian limiting behavior from eqs (17) and (18) once *G* is known (*G* can be determined independently at low scan rates, *vide infra*). I_0 has a given value for the system at constant temperature and can be calculated from the current under dark conditions. Once $I_{p,rev}$ and I_0 are known I_L can be calculated from θ using eq (23). The shape of the voltammograms is affected by changes on

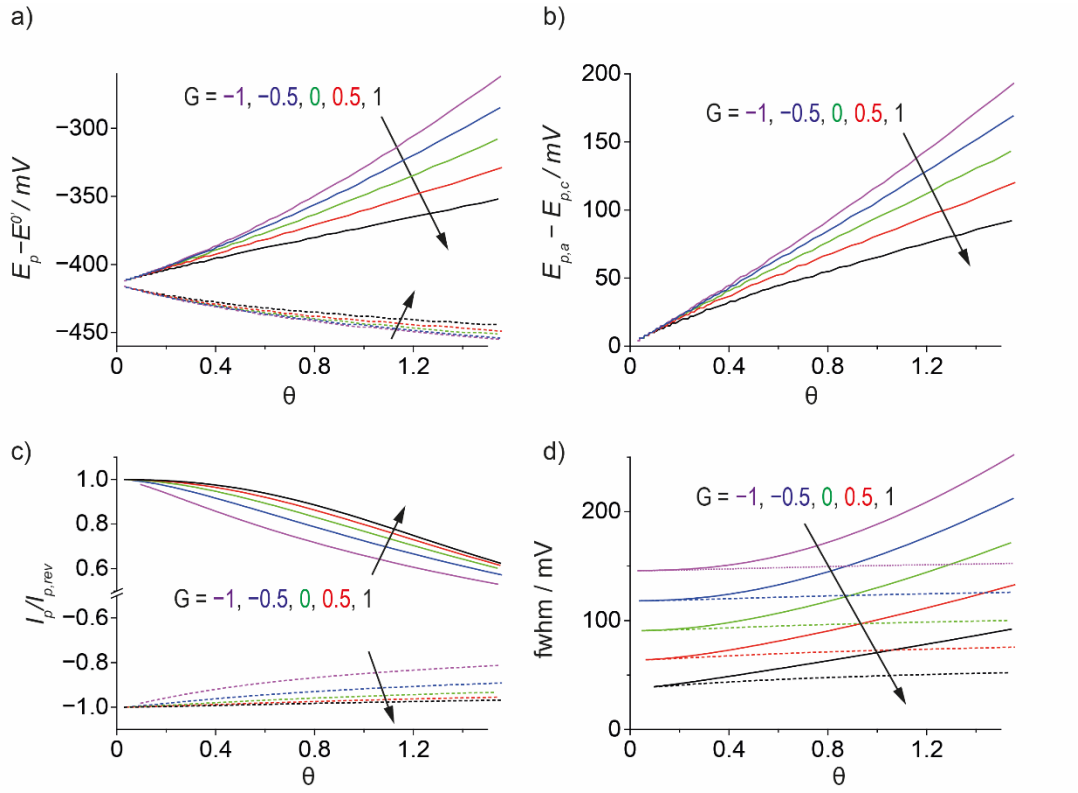

Figure 2. Dependence of the diode parameter θ on the voltammogram shape for different G values under infinite kinetics. The voltammogram shape is defined by the (a) peak potentials, (b) peak separation, (c) peak current, and (d) fwhm. The solid and dashed lines are for the anodic and cathodic waves, respectively, and for different G values (G = −1 (magenta line), G = −0.5 (blue line), G = 0 (green line), G = 0.5 (red line) and G = 1 (black line)). I_0 is set to 10^{-6} mA, and I_L to 10 mA.

θ, as shown by the curves in Figure 1b. Figure 2 summarizes the effect of changes on θ on the characteristic features of the current–potential curves, for different values of G and under infinite kinetics. Namely, Figure 2 shows the effect of θ on peak potentials (E_p, Figure 2a), peak separation ($E_{p,a}$−$E_{p,c}$, Figure 2b), peak currents (I_p, as denoted in general from now on, Figure 2c), and on values of full width at half maximum (fwhm, Figure 2d). As discussed above, for a photoanode the anodic peak is affected more than the cathodic peak (and the opposite for a photocathode). It is noteworthy that an increase on θ splits the positions of the anodic peak respect to the cathodic peak (Figure 2b). This type of peak-to-peak separation is therefore purely a semiconductor effect, as it can be completely associated to changes in θ and is not related to electron transfer kinetics. This is in contrast with monolayers attached on metallic electrodes where the magnitude of peak separation is an indication of the electron transfer kinetics and from which the kinetic constant $k_{et,ap}$ is estimated.[10] The immediate consequence of the peak separation when observed in semiconductor electrodes is that it will be wrongly attributed to a kinetic effect and interpreted as a slow electron transfer. We believe this is a commonly encountered error in the literature, which in most cases reports slower kinetic values for semiconducting systems.[9] We argue that the slower kinetics reported for semiconductors, compared against metals, might be at least in part, a misconception. Voltammetric waves in semiconductors can be separated because the diode character of the electrode, and not because a low value of $k_{et,ap}$. For an accurate kinetic analysis of a diffusionless redox process at a semiconductor/liquid interfaces it is therefore very important to be able to separate kinetic from diode effects. It is also key to note that the self-interaction parameter, G, affects not only I_p and fwhm (Figure 2c and d), as expected also for a metal electrode, but has also an influence on the peak-to-peak separation (Figure 2b).

Figure 3 shows two voltammetric waves simulated under finite kinetics and in absence of interactions (G = 0) using the model developed in the previous section. Both voltammetric curves show equal electron transfer kinetics ($k_{et,ap}$ = 1.0 s^{-1}), but one takes into account the semiconductor nature of the electrode (symbols), while the other doesn't (solid line). It is clear that part of the peak separation in the voltammograms in Figure 3 (symbols) is due to the diode nature of the electrode and not to its electron transfer kinetics. If $k_{et,ap}$ is calculated (symbols) using the Laviron model for a metal

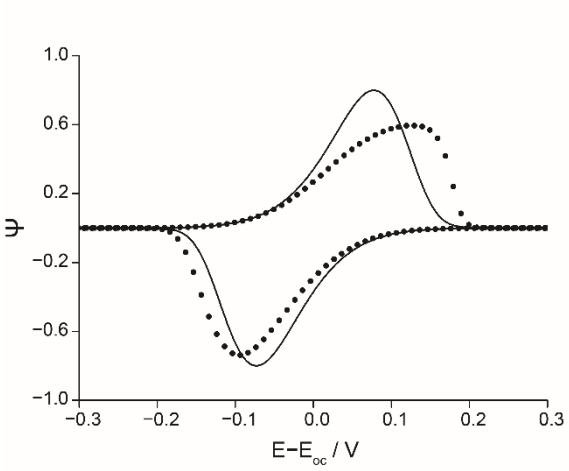

Figure 3. Semiconductor versus metallic electrode under same kinetics. Simulated cyclic voltammetry curves for a metallic electrode (solid line) and for a semiconductor electrode in the presence of diode effects (symbols, θ = 0.7). Sweep rate is 0.1 V/s, α is 0.5 and $k_{et,ap}$ is set to1 s^{-1}.

electrode,[10] the obtained value ($k_{et,ap}$ = 0.2 s^{-1}) is one order of magnitude lower than the actual one ($k_{et,ap}$ = 1.0 s^{-1}). From this theoretical example it can be concluded that a correct kinetic analysis for redox couples tethered at a semiconductor/liquid interface requires considering the diode-like nature of the electrode.

Figure 4 shows the influence of $k_{et,ap}$ on the peak parameters (E_p, ΔE_p, I_p and fwhm) at different values of θ and in the absence of interactions (G = 0). Figure S1 (Supporting Information) shows this plot for different values of G. These plots can be used to get a rough estimation of $k_{et,ap}$, however a complete simulation analysis is recommended due to the complexity of the process, i.e. the presence of interdependent factors such as kinetics, interactions and diode effects. As can be seen in Figure 4, there are three clear regions corresponding to very fast (Nernstian, $\log \bar{k}_{et,ap} \geq 1$), quasi-reversible $\left(-1.5 \leq \log \bar{k}_{et,ap} < 1\right)$ and fully irreversible $\left(\log \bar{k}_{et,ap} < -1.5\right)$ charge transfer reactions. Moreover, in absence of interaction effects on the voltammograms, the evolution of the peak parameters with $\bar{k}_{et,ap}$ is qualitatively the same, regardless the value of θ. As

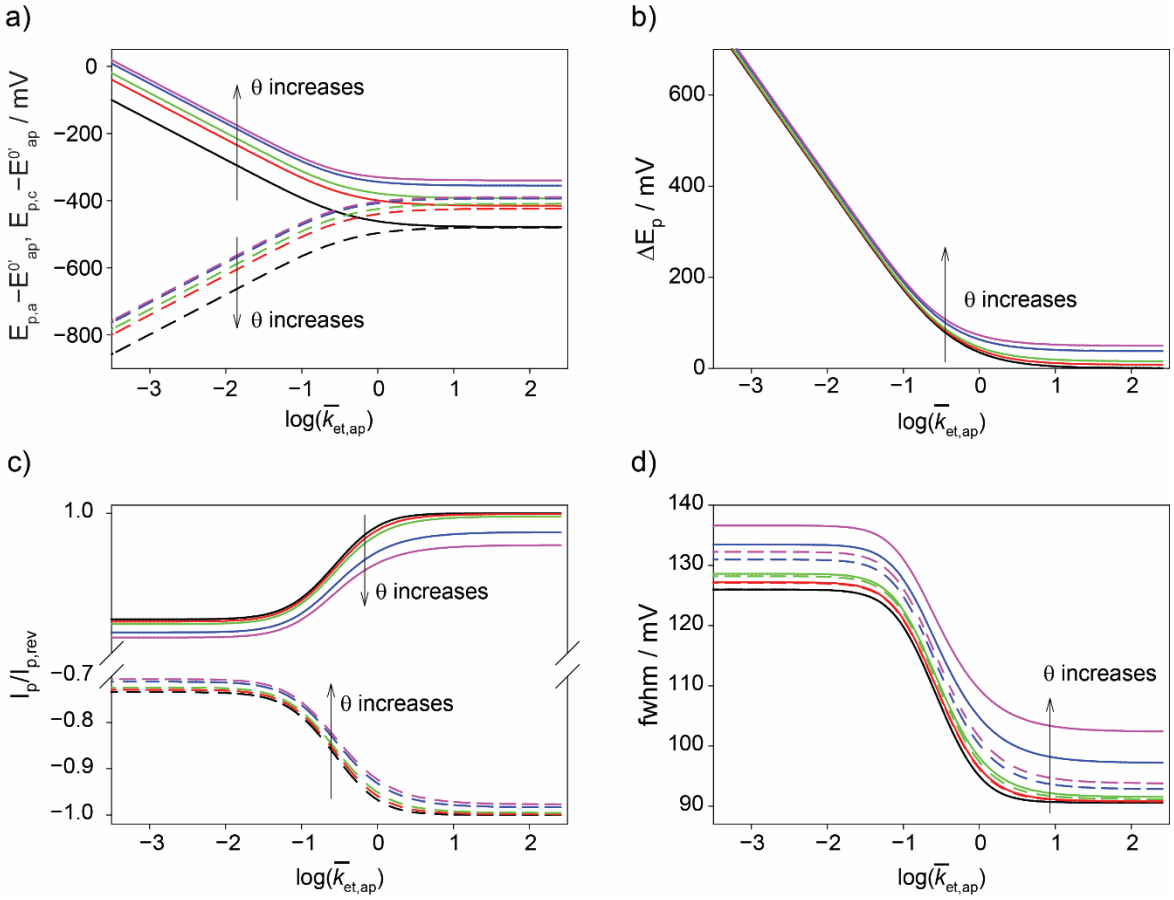

Figure 4. Dependence of the electron transfer kinetics k_{et} on the voltammogram shape in the presence of diode effects θ (photoanode) and in the absence of lateral interactions. (a) E_p vs $k_{et,ap}$ (b) ΔE_p vs $k_{et,ap}$. (c) I_p vs $k_{et,ap}$. (d) fwhm vs $k_{et,ap}$ The values of θ for the different curves are: $7.8 \cdot 10^{-3}$ (black lines), $7.8 \cdot 10^{-2}$ (red lines), 0.156 (green lines), 0.389 (blue lines) and 0.519 (pink lines). The sweep rate is 100 mV s^{-1}, α is 0.5 and $G = s$ = 0. Solid lines corresponds to the direct (anodic scan) and dashed lines for the reverse (cathodic one).

stated above, in the Nernstian region, the increase of θ leads to a decrease of the anodic peak current much more marked than that observed for the cathodic one (the opposite is true for a photocathode).

For the above mentioned example not to remain a theoretical exercise we developed an experimental model by attaching a ferrocene monolayer on an amorphous silicon semiconductor electrode by a previously reported method[20] (see scheme in Figure 5a). The amorphous silicon was deposited on either an n-type or a p-type crystalline silicon. The doping type of the crystalline substrate determines the photoanode (n-type) or photocathode (p-type) behaviour of the electrode. In practice, the challenge when interpreting cyclic voltammetric curves remains in distinguishing and isolating kinetic effects, defined by $k_{et,ap}$, from semiconductor effects, defined by θ, and electrostatic interactions, defined by G. Bringing changes to θ without affecting $k_{et,ap}$ would allow decoupling one effect from the other. From the parameters that affect θ, I_L can be easily and predictably changed by changing the intensity of the light on the semiconductor. Moreover, I_L in theory is not dependent on $k_{et,ap}$ (see the previous section) and is linearly dependent on the light intensity[18,21] (Figure S2, Supporting Information). Therefore, the light intensity can be assumed to not affect the electron transfer kinetics in the system here studied, and then θ can be adjusted by studying the voltammograms at different light intensity. Figure 5b shows cyclic voltammograms taken at different light intensity (solid lines) and their fittings (symbols). Table S1 (Supporting Information) resumes the parameters used for these fittings. Once the semiconductor θ parameter is known, the electron transfer rate constant $k_{et,ap}$ can be obtained by studying the influence of the voltammetric curves with the scan rate v, as shown in Figure 5c. The parameters used for these fittings are listed in Table S2 (Supporting Information).

For instance, considering our experimental data, the error that one would make by using a "metallic" model to calculate rate constants in a semiconductor would be close to 81%. For a photoanode operating at the highest light intensity, *i.e.* when diode effects are less notable, the value of $k_{et,ap}$ refined using Laviron's equations is more than 5 times lower than the value obtained with our model to account for diode effects (14 vs 75 s^{-1}). The $k_{et,ap}$ value of 75 s^{-1} is in accordance with literature values reported for highly doped semiconductor electrodes.[22,23,24] The Laviron model underestimates the electron transfer constant, wrongly sensing a slower electron transfer than the actual one as a consequence of the potential drop across the semiconductor space charge layer. If the Laviron model is applied at the low-

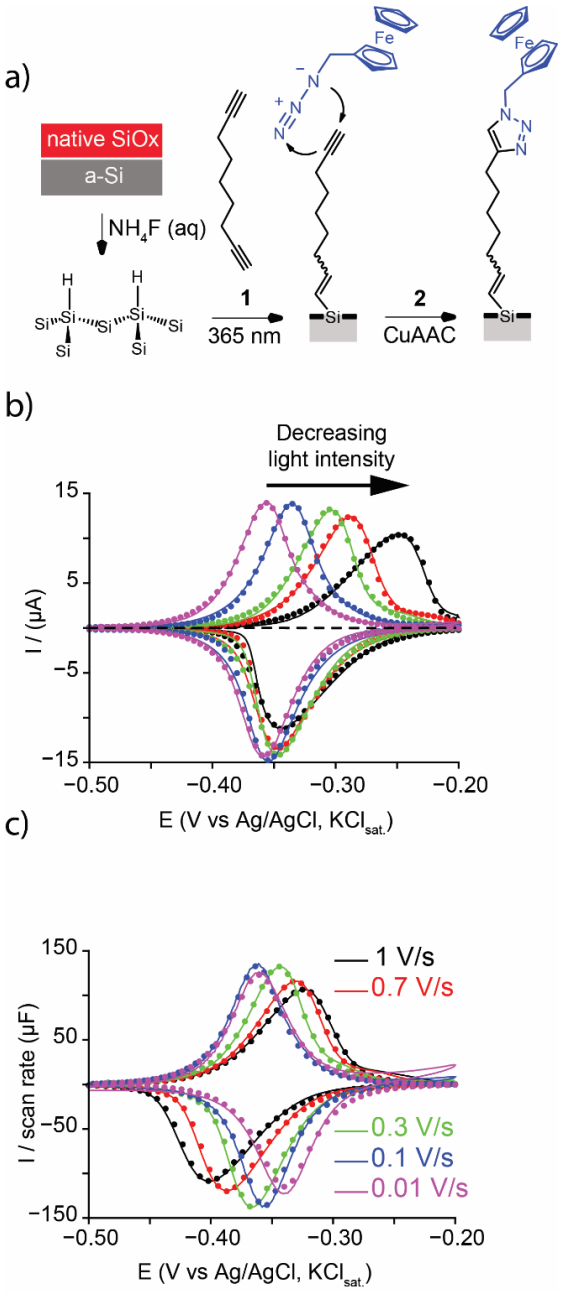

Figure 5. Photoanode systems. (a) Light-assisted hydrosilylation of 1,8-nonadiyne **1** at a Si–H electrode and attachment of azidomethylferrocene **2** via CuAAC reactions to yield redox-active monolayers. (b) Experimental (solid lines) and fitted (symbols) cyclic voltammograms (0.1 Vs^{-1}) taken at different light intensities (1, 2, 4, 11 and 27 mW cm^{-2}). (c) Experimental (solid lines) and fitted (symbols) cyclic voltammograms taken at different scan rates under illumination (27 mW cm^{-2}). In the fittings, k_{et} and G are assumed to be independ on light intensity. Best fits values are $k_{et,\,ap}$ = 75 s^{-1}, G = 0.8, $I_0 = 10^{-5}$ A, $I_{L,a}$ = 750 μA, $I_{L,c}$ = 250 μA, s = −1 and α was set to 0.5. For the light intensity study, we introduce a correction factor, f_I, such that the values of $I_{L,a}$ and $I_{L,c}$ are now ($f_I \times I_{L,a}$) and ($f_I \times I_{L,c}$) with $0 < f_I < 1$ (a value of 1 corresponds to full illumination, and 0 to no light). The obtained values of f_I are 0.05, 0.125, 0.20, 0.55 and 1 for 1, 2, 4, 11 and 27 mW·cm^{-2}, respectively. Electrolyte is 1.0 M $HClO_4$.

est light intensity the calculated electron transfer constant is 75 times lower ($k_{et,ap}$ = 1 s^{-1}) than the one obtained applying the model we developed here. Moreover, the Laviron model would wrongly suggest that kinetics depends upon light intensity. It is likely that values reported in literature have similar errors because of the semiconductor nature of the electrode. It is well known that electron transfer constants reported for semiconductor silicon electrodes systematically show a smaller electron transfer compared to gold electrodes.[9] This has been attributed to differences in the electronic coupling between the attached molecules and the surface and density of states. Our results show that the slower electron transfer for semiconductor electrodes, compared to metallic electrodes, is at least in part a consequence of using a model not applicable to semiconductors.

The introduction of the Frumkin isotherm in the model allows to sense electrostatic interactions experimented by the attached electroactive molecules.[11] Interactions have been broadly observed in the literature,[9] with the fwhm being broader or narrower than the theoretical 90.6 mV for a Nernstian process, indicating repulsive or attractive forces, respectively. The degree of interaction is accounted through the G parameter, where $G < 0$ is indicative of repulsions and $G > 0$ attractions, and directly related to the fwhm in a Nernstian process and a metallic electrode.[11] However, under finite kinetics and diode effects, the fwhm is not only a function of G, but also of θ and k_{et} as shown in Figures 2d and 4d, respectively. Therefore, for the determination of G one needs to ensure that kinetic and diode effects are not present by moving to the part of the graphs of Figures 2d and 4d where fwhm does not depend neither on $k_{et,ap}$ nor on θ. For practical situations this criteria is met when $-\log \theta > 1.3$ and dimensionless rate constants $k_{et,ap}$ >3 s^{-1}, which in the experimental model we have here studied corresponds to scan rates of $v < 100$ mV·s^{-1} for a true rate constant in the range 1–10 s^{-1} using the highest light intensity (Figure S3, Supporting Information).

The model is also applicable to photocathodes (*vide supra* in "Development of the analytical model"), and Figure S4 (Supporting Information) shows for experimental voltammetric curves (solid lines) and fittings (symbols) for ferrocene monolayers on p-type electrodes operating under different light intensities (panel a) and scan rates (panel b). Tables S3 and S4 (Supporting Information) list the fitting parameters.

CONCLUSIONS

In summary, we have developed a theoretical model that allows determining quantitatively the electron transfer constant of strongly adsorbed electroactive monolayers at semiconductor photoelectrodes and describes the shapes of experimentally encountered cyclic voltammetry curves. This model expands previous work developed by Laviron[10,11] and Santangelo et al.[12] and will aid the kinetic analysis of redox reactions at chemically modified semiconductor electrodes. The model is intended to lead the advancement in the fields of energy production and storage and light-addressable electrochemistry.[25] It is also of relevance to the field of molecular electronics: silicon has just entered this area with STM single-molecule break-junctions experiments made technically possible in 2017.[26] To date, reported kinetic values of these systems show slower electron transfer kinetics than metals, which we argue it is most likely to be due to an inaccurate analysis of the voltammetric curves. The implication of the findings here reported are that for an accurate description of the electron transfer of electroactive species attached at semiconductors require the use of a model that describes accurately the potential distribution at the semiconductor/electrolyte interface.

We have described a step-by-step analytical procedure to separate diode currents, kinetic rate constants and intermolecular interaction parameters by adjusting light intensity and scan rates during cyclic voltammetry experiments on semiconducting electrodes. At strong illumination and slow scan rates, fwhm values are independent of the diode-related θ parameter and the Frumkin interaction parameter G can be obtained. At slow scan rates the peak separation is independent of the rate constant and θ can be obtained by analysing data recorded at different light intensities. Finally, once G and θ are known, the electron transfer rate constant is obtained through a scan rate study at high light intensity.

AUTHOR INFORMATION

Corresponding Authors

*Email: simone.ciampi@curtin.edu.au
*Email: josquin@um.es

ACKNOWLEDGMENT

This work was financially supported by the Australian Research Council (DP190100735). A.M. and J.G. greatly appreciate the financial support provided by the Fundación Séneca de la Región de Murcia (Project 19887/GERM/15) as well as by the Ministerio de Economía y Competitividad (Projects CTQ-2015-65243-P). We thank Vinicius R. Gonçales and J. Justin Gooding for the preparation and generous supply of amorphous silicon substrates.

ASSOCIATED CONTENT

Supporting Information

The Supporting Information is available free of charge on the ACS Publications website at DOI:

Detailed experimental procedure for surface modification; chemicals and material used; theoretical dependence of k_{et} and G on voltammogram shape; experimental dependence of I_L with light intensity; parameters used for the fittings; theoretical dependence of fwhm on θ at different values of G (PDF).

REFERENCES

(1) Braun, F. Ueber die Stromleitung durch Schwefelmetalle. *Ann. Phys. (Berlin, Ger.)* **1875**, *229*, 556-563.

(2) https://www.cadence.com/content/cadence-www/global/en_US/home/company/newsroom/press-releases/pr/2018/imec-and-cadence-tape-out-industry-s-first-3nm-test-chip.html (accessed: January 2019)

(3) Bard, A. J. Design of Semiconductor Photoelectrochemical Systems for Solar Energy Conversion. *J. Phys. Chem. C* **1982**, *86*, 172-177.

(4) Sun, K.; Shen, S.; Liang, Y.; Burrows, P. E.; Mao, S. S.; Wang, D. Enabling Silicon for Solar-Fuel Production. *Chem. Rev.* **2014**, *114*, 8662-8719.

(5) Henderson, M. A. A Surface Science Perspective on TiO_2 Photocatalysis. *Surf. Sci. Rep.* **2011**, *66*, 185-297.

(6) Chen, D.; Zhang, H.; Li, X.; Li, J. Biofunctional Titania Nanotubes for Visible-Light-Activated Photoelectrochemical Biosensing. *Anal. Chem.* **2010**, *82*, 2253-2261.

(7) Zhao, W.-W.; Xu, J.-J.; Chen, H.-Y. Photoelectrochemical Immunoassays. *Anal. Chem.* **2018**, *90*, 615-627.

(8) Lewis, N. S. Chemical Control of Charge Transfer and Recombination at Semiconductor Photoelectrode Surfaces. *Inorg. Chem.* **2005**, *44*, 6900-6911.

(9) Fabre, B. Functionalization of Oxide-Free Silicon Surfaces with Redox-Active Assemblies. *Chem. Rev.* **2016**, *116*, 4808-4849.

(10) Laviron, E. General Expression of the Linear Potential Sweep Voltammogram in the Case of Diffusionless Electrochemical Systems. *J. Electroanal. Chem. Interfacial Electrochem.* **1979**, *101*, 19-28.

(11) Laviron, E.; Roullier, L. General Expression of the Linear Potential Sweep Voltammogram for a Surface Redox Reaction with Interactions between the Adsorbed Molecules: Applications to Modified Electrodes. *J. Electroanal. Chem. Interfacial Electrochem.* **1980**, *115*, 65-74.

(12) Santangelo, P. G.; Miskelly, G. M.; Lewis, N. S. Cyclic Voltammetry at Semiconductor Photoelectrodes. 1. Ideal Surface-Attached Redox Couples with Ideal Semiconductor Behavior. *J. Phys. Chem.* **1988**, *92*, 6359-6367.

(13) Nerngchamnong, N.; Thompson, D.; Cao, L.; Yuan, L.; Jiang, L.; Roemer, M.; Nijhuis, C. A. Nonideal Electrochemical Behavior of Ferrocenyl–Alkanethiolate SAMs Maps the Microenvironment of the Redox Unit. *J. Phys. Chem. C* **2015**, *119*, 21978-21991.

(14) Zhang, L.; Vogel, Y. B.; Noble, B. B.; Gonçales, V. R.; Darwish, N.; Brun, A. L.; Gooding, J. J.; Wallace, G. G.; Coote, M. L.; Ciampi, S. TEMPO Monolayers on Si(100) Electrodes: Electrostatic Effects by the Electrolyte and Semiconductor Space-Charge on the Electroactivity of a Persistent Radical. *J. Am. Chem. Soc.* **2016**, *138*, 9611-9619.

(15) Vogel, Y. B.; Zhang, L.; Darwish, N.; Gonçales, V. R.; Le Brun, A.; Gooding, J. J.; Molina, A.; Wallace, G. G.; Coote, M. L.; Gonzalez, J.; Ciampi, S. Reproducible Flaws Unveil Electrostatic Aspects of Semiconductor Electrochemistry. *Nat. Commun.* **2017**, *8*, 2066.

(16) Gonzalez, J.; Sequí, J.-A. Kinetic Implications of the Presence of Intermolecular Interactions in the Response of Binary Self-Assembled Electroactive Monolayers. *ACS Omega* **2018**, *3*, 1276-1292.

(17) Uosaki, K.; Sato, Y.; Kita, H. Electrochemical Characteristics of a Gold Electrode Modified with a Self-Assembled Monolayer of Ferrocenylalkanethiols. *Langmuir* **1991**, *7*, 1510-1514.

(18) Peter, L. M. Dynamic Aspects of Semiconductor Photoelectrochemistry. *Chem. Rev.* **1990**, *90*, 753-769.

(19) Gerischer, H. Electrochemical Behavior of Semiconductors Under Illumination. *J. Electrochem. Soc.* **1966**, *113*, 1174-1182.

(20) Ciampi, S.; Eggers, P. K.; Le Saux, G.; James, M.; Harper, J. B.; Gooding, J. J. Silicon (100) Electrodes Resistant to Oxidation in Aqueous Solutions: An Unexpected Benefit of Surface Acetylene Moieties. *Langmuir* **2009**, *25*, 2530-2539.

(21) Bube, R. H. Saturation of Photocurrent with Light Intensity. *J. Appl. Phys.* **1960**, *31*, 1301-1302.

(22) Ciampi, S.; Choudhury, M. H.; Ahmad, S. A. B. A.; Darwish, N.; Brun, A. L.; Gooding, J. J. The Impact of Surface Coverage on the Kinetics of Electron Transfer through Redox Monolayers on a Silicon Electrode Surface. *Electrochim. Acta* **2015**, *186*, 216-222.

(23) Mishchenko, A.; Abdualla, M.; Rudnev, A.; Fu, Y.; Pike, A. R.; Wandlowski, T. Electrochemical Scanning Tunnelling Spectroscopy of a Ferrocene-Modified n-Si(111)-Surface: Electrolyte Gating and Ambipolar FET Behaviour. *Chem. Commun.* **2011**, *47*, 9807-9809.

(24) Ciampi, S.; Luais, E.; James, M.; Choudhury, M. H.; Darwish, N. A.; Gooding, J. J. The Rapid Formation of Functional Monolayers on Silicon Under Mild Conditions. *Phys. Chem. Chem. Phys.* **2014**, *16*, 8003-8011.

(25) Choudhury, M. H.; Ciampi, S.; Yang, Y.; Tavallaie, R.; Zhu, Y.; Zarei, L.; Gonçales, V. R.; Gooding, J. J. Connecting Electrodes with Light: One Wire, Many Electrodes. *Chem. Sci.* **2015**, *6*, 6769-6776.

(26) Aragonès, A. C.; Darwish, N.; Ciampi, S.; Sanz, F.; Gooding, J. J.; Díez-Pérez, I. Single-Molecule Electrical Contacts on Silicon Electrodes under Ambient Conditions. *Nat. Commun.* **2017**, *8*, 15056.